Light-induced electrons suppressed by Eu^{3+} ions doped in $Ca_{11.94-x}Sr_xAl_{14}O_{33}$ caged phosphors for LED and FEDs

Bian, H.; Liu, Y.; Yan, D.; Zhu, H.; Liu, C.; Xu, C.; Wang, X.; Zhang, H.

DOI
10.1111/jace.14866

Publication date
2017

Document Version
Final published version

Published in
Journal of the American Ceramic Society

Received: 21 December 2016 | Accepted: 22 February 2017

DOI: 10.1111/jace.14866

ORIGINAL ARTICLE

Journal of the American Ceramic Society

Light-induced electrons suppressed by Eu^{3+} ions doped in $Ca_{11.94-x}Sr_xAl_{14}O_{33}$ caged phosphors for LED and FEDs

Hongyu Bian[1] | Yuxue Liu[1] | Duanting Yan[1] | Hancheng Zhu[1] | Chunguang Liu[1] | Changshan Xu[1] | Xiaojun Wang[2] | Hong Zhang[3]

[1]School of physics, Northeast Normal University, Changchun, China

[2]Department of Physics, Georgia Southern University, Statesboro, Georgia

[3]Van't Hoff Institute for Molecular Sciences, University of Amsterdam, Amsterdam, The Netherlands

Correspondence
Yuxue Liu, School of physics, Northeast Normal University, Changchun, China.
Email: yxliu@nenu.edu.cn
and
Hong Zhang, Van't Hoff Institute for Molecular Sciences, University of Amsterdam, Amsterdam, The Netherlands.
Email: H.Zhang@uva.nl

Funding information
National Natural Science Foundation of China, Grant/Award Number: 11374047, 11674050, 11304036; European union MSCA-ITN-2015-ETN Action program, ISPIC, Grant/Award Number: 675742; Netherlands Organisation for Scientific Research in the framework of the Fund New Chemical Innovation (2015) TA, Grant/Award Number: 731.015.206.

Abstract

Control of light-induced electron generation is of vital importance for the application of caged phosphors. For Eu-doped $Ca_{11.94-x}Sr_xAl_{14}O_{33}$ caged phosphors, the suppressed effect of strontium doping on the light-induced electrons is observed compared to the europium-free $Ca_{11.94-x}Sr_xAl_{14}O_{33}$ phosphors. In the presence of europium ions, Sr doping will promote the reduction of Eu^{3+} to Eu^{2+}. The Rietveld refinement suggests that unit cell volumes of the $Ca_{11.94-x}Sr_xAl_{14}O_{33}$:$Eu_{0.06}$ samples are expanded when Ca^{2+} ions are replaced by Sr^{2+} ions. The absorption and FTIR transmittance spectra confirm that the competitive reaction of encaged O^{2-} anions with H_2 is suppressed. For the sample (x=0.48), the higher thermal activation energy (~0.40 eV) for luminescence quenching can be attributed to the more rigid framework structure after Sr doping. For $Ca_{11.94-x}Sr_xAl_{14}O_{33}$:$Eu_{0.06}$ phosphors, their emission colours are tuned from red to purple upon 254 nm excitation and from pink to blue under electron beam excitation through Sr substitution. The insight gained from this work may have a significant guiding to design new phosphors for LED and FEDs and novel nanocaged mutifunctional materials.

KEYWORDS
luminescence, rare earths, C12A7

1 | INTRODUCTION

Inorganic and organic caged compounds have attracted more attentions and exhibited many potential applications due to their unique physical and chemical properties.[1-3] For example, mayenite ($Ca_{12}Al_{14}O_{33}$) is one kind of such multifunctional materials exhibiting its variety of possible applications, such as catalytic[4], electronic devices,[5] sensors,[6] solid electrolytes[7], and electrides.[8,9] These functions are related to its special nanocage structure, as shown in Figure 1A. Its unit cell is expressed as $[Ca_{24}Al_{28}O_{64}]^{4+}$:$2O^{2-}$, which consists of a positively charged lattice framework and two encaged O^{2-} ions, occupying the two cages of the twelve cages.[10] Usually, encaged electrons, OH^-,[11] H^-,[12-14] Cl^-,[15] F^-,[15] CN^-,[16] will substitute for encaged O^{2-} anions after the samples treated under different conditions. In particular, for the application of encaged electrons, Hayashi et al. reported that the C12A7:H^- sample can be changed from an insulator to a conductor for a transparent circuit because of the existence of light-induced electrons after UV-light irradiation.[12]

On the other hand, the reported study showed that $Sr_{12}Al_{14}O_{33}$ (S12A7) has a similar structure to $Ca_{12}Al_{14}O_{33}$ and a larger lattice constant (a=1.233 nm) than $Ca_{12}Al_{14}O_{33}$ (a=1.199 nm).[17] According to the above results, Zhang et al. found that Sr doping in Gd^{3+}-doped $Ca_{12(1-x)}Sr_{12x}Al_{14}O_{33}$ powders could give rise to the enhancement of the exchange, formation and annihilation of various encaged anions.[18] Thus, the numbers of encaged H^-, OH^- anions and electrons

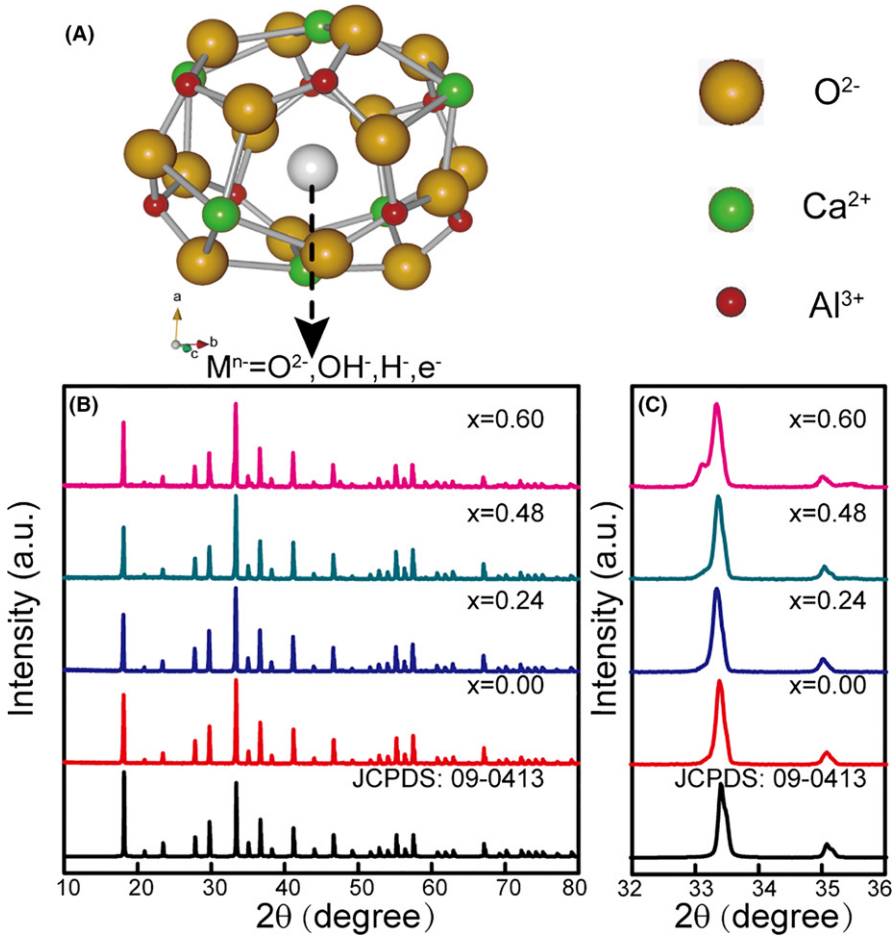

FIGURE 1 (A) The nanocage structure of $Ca_{12}Al_{14}O_{33}$, (B) XRD and (C) the magnifying XRD patterns of $Ca_{11.94-x}Sr_xAl_{14}O_{33}:Eu_{0.06}$ (x=0.00, 0.24, 0.48 and 0.60) powders annealed in H_2 atmosphere [Color figure can be viewed at wileyonlinelibrary.com]

created by UV-light irradiation increased with increasing the amount of Sr in the presence of the stable trivalent rare earth ions like Gd^{3+} ion. Meanwhile, since more encaged OH^- anions were produced after Sr doping, the lower luminescent intensity of the lanthanide-doped phosphor can be observed. However, in the case of the unstable trivalent rare earth ions such as Eu^{3+} ion, it is still a challenge to understand how Sr doping affects the formation of encaged electrons and modulates the luminescence of unstable rare-earth ions. On the other hand, not only Eu^{3+} ions are used as a luminescent probe in many fields, including structural probe, detection of medicine and physiological range,[19-24] but also Eu^{3+} and Eu^{2+} are good emission centers in phosphors for white LEDs and displays.[25-31] Meanwhile, the Eu^{3+} can be reduced to Eu^{2+} in H_2 atmosphere, which may influence the exchange of anions. This understanding will benefit for designing functional materials and novel phosphors for lighting and displays.

In this work, Eu-doped $Ca_{11.94-x}Sr_xAl_{14}O_{33}$ phosphors with different Sr dopant amounts have been synthesized by self-propagating combustion method followed by thermal annealing in H_2 atmosphere. The suppressed effect of strontium doping on the light-induced electrons can be observed compared to the europium-free sample. In the presence of Eu^{3+}, Sr doping can facilitate the exchange of encaged anions and promote the reduction of Eu^{3+} to Eu^{2+} in $Ca_{11.94-x}Sr_xAl_{14}O_{33}$ phosphors. For the $Ca_{11.94-x}Sr_xAl_{14}O_{33}:Eu_{0.06}$ phosphors, the changes in emission colors with different excitation sources are observed (from red to purple upon 254 nm excitation and from pink to blue under electron beam excitation). The insight gained from this work may have the potential applications in designing new phosphors and related devices for LED and FEDs and developing nanocaged multifunctional materials.

2 | EXPERIMENTAL PROCEDURE

$Ca_{11.94-x}Sr_xAl_{14}O_{33}:Eu^{3+}{}_{0.06}$($x$=0.00, 0.24, 0.48 and 0.60) powders were prepared by self-propagating combustion method. Here, for each of the samples with different Sr-doping concentrations, the Eu^{3+}-doping concentration is the same and set at 0.06, which was acquired by optimizing the microstructure and luminescence of Eu^{3+}-doped $Ca_{12}Al_{14}O_{33}$. A mixture of aluminum nitrate (99.99%), strontium nitrate (99.99%), calcium nitrate (99.99%), europium nitrate (99.99%), β-alanine and urea was dissolved in deionized water based on the nominal metal mole ratio in

$Ca_{11.94-x}Sr_xAl_{14}O_{33}:Eu^{3+}{}_{0.06}$. After the precursor solution in a cylinder-shaped container was changed into a yellow-white gel, it was put into a preheated furnace. Then the solvent was vaporized, the spontaneous ignition happened and the pale-white ashes were acquired. Subsequently, these ashes were calcined at 1000°C in air for 6 hours to eliminate carbon and nitrogen residues remaining in the powders. Finally, the calcined $Ca_{11.94-x}Sr_xAl_{14}O_{33}:Eu^{3+}{}_{0.06}$ powders were annealed at 1300°C in a $20\%H_2/80\%N_2$ atmosphere for 3 hours to obtain the final samples with different Sr-doping concentrations.

Crystal structures of europium-doped $Ca_{11.94-x}Sr_xAl_{14}O_{33}$ powders were examined by a Rigaku D/max-RA X-ray diffraction (XRD) spectrometer, using Cu$K\alpha$ radiation (line of 0.15418 nm). Energy dispersive X-ray spectroscopy (EDX) spectra and morphology of the samples were performed by means of a scanning electron microscope (SEM, Quanta FEG 250, FEI Corporate, Hillsboro, OR). Photoluminescence (PL), emission and excitation spectra were recorded with a RF-5301PC, Shimadzu, Kyoto, Japan spectrofluorometer. Fourier Transform IR (FTIR) transmittance spectra were taken with a Nicolet 6700 Fourier Transform Infrared Spectrometer. $Ca_{11.94-x}Sr_xAl_{14}O_{33}:Eu_{0.06}$ powders were mixed with KBr at a weight ratio of 3:100 and then ground and pressed at a pressure of 10 MPa to obtain pellets. Absorption spectra were performed, using a UH4150UV/VIS/NIR spectrophotometer (Hitachi, Japan). Luminescence decays were taken with a 600 MHz LeCroy digital oscilloscope from an optical parametric oscillator. Temperature-dependent PL spectra were tested by a SHIMADZU RF-5301PC spectrofluorometer and a temperature controller in house. Cathodoluminescence (CL) measurement was performed, using a Mono CL4 system (Gatan UK) attached to an SEM, in which the phosphors were excited by an electron beam (accelerating voltage ≤5 kV, filament current=154 μA). All measurements except the temperature-dependent PL were performed at room temperature.

3 | RESULTS AND DISCUSSION

XRD patterns of $Ca_{11.94-x}Sr_xAl_{14}O_{33}:Eu_{0.06}$ powders with different Sr-doping concentrations are shown in Figure 1B. For the samples with Sr-doping concentration lower than 0.60, it can be observed that all diffraction peaks can be confirmed by those of single-phase $Ca_{12}Al_{14}O_{33}$ powders (JCPDS: 09-0413). This indicates that single-phased Sr and Eu co-doped $Ca_{12}Al_{14}O_{33}$ is obtained. When the Sr-doping concentration is equal to 0.60, the impurity phase, $Ca_3Al_2O_6$, emerges. Since Eu^{3+} (0.95 Å) and Sr^{2+} (1.12 Å) have a similar ionic radius to Ca^{2+} (0.99 Å) and a larger one than Al^{3+} (0.39 Å), it is reasonable to show that Ca^{2+} ions were replaced by Eu^{3+} and Sr^{2+} in $Ca_{11.94-x}Sr_xAl_{14}O_{33}:Eu_{0.06}$. It can also be noted that the diffraction peak at 33.3°C shifts toward the lower diffraction angle side, as shown in Figure 1B,C, as the Sr-doping concentration increases. This can be explained by the unit cell volume expansion of $Ca_{11.94-x}Sr_xAl_{14}O_{33}:Eu_{0.06}$ owing to the replacement of Ca^{2+} ions by larger Sr^{2+} ions in $Ca_{12}A_{14}O_{33}$ host lattice.[31]

To further demonstrate Sr dopant amount, expand the unit cell volume of the samples, XRD patterns of the undoped (x=0.00) and Sr-doped samples (x=0.24, 0.48) were defined by GSAS II refinement.[32] The experimental and calculated XRD profiles and Bragg positions and their differences for the Rietveld refinement at room temperature are shown in Figure 2A. The space groups, cell parameters and reliability factors are summarized in Table 1. It can be found that the undoped $Ca_{12}Al_{14}O_{33}$:Eu exhibits a cubic phase with space group $I\bar{4}3d$ and $a=b=c$=11.976 Å, V=1717. 924 Å^3, $\alpha=\beta=\gamma=90°$. All the atom positions, fraction factors and thermal vibration parameters were refined by convergence and satisfied well with the reflection conditions, weighted profile R-factor (R_{wp})=11.70%, the integrated intensity R-factor ($R_F{}^2$)=3.59%, and goodness of fit χ^2=2.14. For the Sr-doped sample (x=0.48), the obtained parameters are $R_F{}^2$=9.56%, R_{wp}=10.77%, and χ^2=1.97. It can be noted that the lattice constant a increases from 11.976 Å (x=0.00) to 11.980 Å (x=0.48) and the unit cell volume V increases as the Sr dopant amount rises. This result indicates that the nanocage size of the Sr-doped sample indeed becomes larger than that of the undoped sample, which is consistent with that reported by Miyakawa et al.[17]

To confirm the composition of the samples, EDX spectra and morphologies of $Ca_{11.94-x}Sr_xAl_{14}O_{33}:Eu_{0.06}$ powders are given in Figure 2B. For the undoped sample (x=0.00), O, Al and Ca elements can be observed. For the doped samples, the calculated Sr dopant amounts are 0.24 and 0.53, respectively, which are consistent with the nominal dopant amounts of Sr (x=0.24, 0.48). Since Eu dopant amount is low, no obvious Eu peak can be detected. In addition, the grain sizes of the three samples are determined to be in the range of 2-4 μm (Figure 2C), which benefits for producing a compact phosphor screen.

According to the earlier studies, when $Ca_{12}Al_{14}O_{33}$ (C12A7) based phosphors are annealed in a hydrogen atmosphere, encaged O^{2-} will react with hydrogen as described in the following reaction:

$$H_2(gas) + O^{2-}(cage) \xrightarrow{\Delta} H^-(cage) + OH^-(cage) \quad (1)$$

After irradiation with UV light, encaged electrons are created as expressed in the following reaction:

$$H^-(cage) + O^{2-}(cage) + Null(cage) \xrightarrow{UV-irradiation} OH^-(cage) + 2e^-(cage) \quad (2)$$

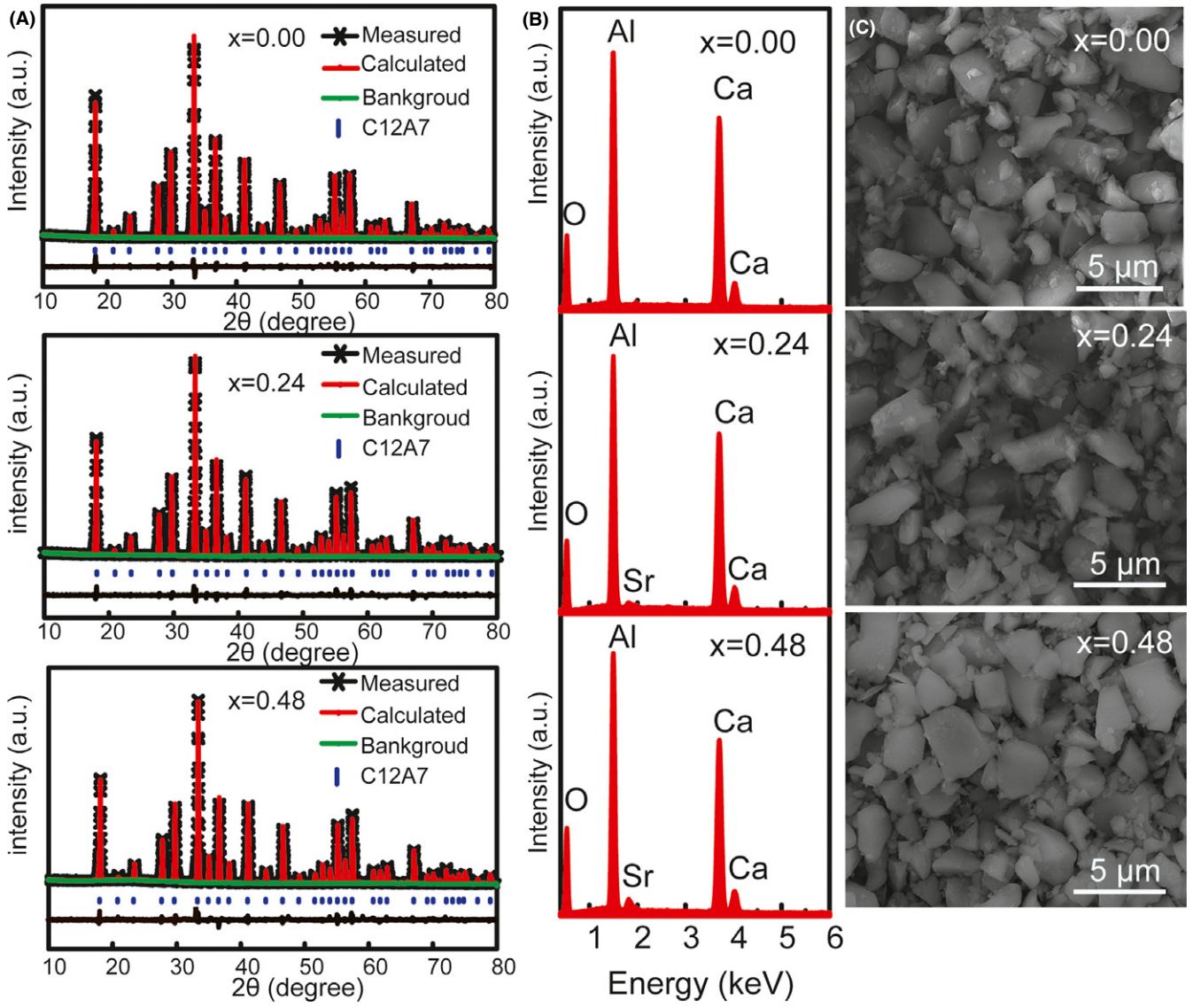

FIGURE 2 (A) The Rietveld refinements of XRD patterns, (B) EDX spectra and (C) SEM images for $Ca_{11.94-x}Sr_xAl_{14}O_{33}:Eu_{0.06}$ (x=0.00, 0.24, 0.48) powders annealed at 1300°C for 3 h [Color figure can be viewed at wileyonlinelibrary.com]

where *null* stands for an empty cage and cage in the parentheses represents a cage occupied by an anion.[12,33,34] On the basis of our previous studies, when rare earth ions were doped in C12A7 (in the case of Gd^{3+}, Ce^{3+}, Dy^{3+} Tb^{3+} and Sm^{3+}), the surface colors of the phosphors after irradiation by UV light turned into green due to the existence of encaged electrons.[18,35–37] Especially, for Gd^{3+}-doped C12A7, the encaged electron concentration increased with increasing Sr doping. Meanwhile, the luminescence intensity of Gd^{3+} decreases due to the existence of more OH^- with increasing Sr doping.

However, when Eu-doped $Ca_{11.94-x}Sr_xAl_{14}O_{33}$ phosphor is irradiated by UV light, its surface did not turn to green color. This result indicates that fewer encaged electrons are created. The absorption spectra of the $Ca_{11.94-x}Sr_xAl_{14}O_{33}:Eu_{0.06}$ powders with different Sr dopant amounts after UV irradiation are given in Figure 3A. It can be seen that there is an absorption edge for each sample in the range of 2.2-3.0 eV and Sr dopant amounts have little influence on the absorption edge position. While, for Sr^{2+} and Gd^{3+} (the same trivalent rare earth ions and the same electronic structure) co-doped $Ca_{12}Al_{14}O_{33}$ powders after irradiation with ultraviolet light, there is an absorption band about 2.8 eV. In that case, the encaged electron concentration is above 10^{19} cm^{-3} as the Sr-doping concentration is higher than 0.06 (0.5 mol%).[18] However, the encaged electron concentrations of the Sr-doped $Ca_{11.94-x}Sr_xAl_{14}O_{33}:Eu_{0.06}$ samples (x=0.24, 0.48) are about 10^{18} cm^{-3}, which is based on the similar shape of the absorption band to that of the undoped Gd^{3+} and Sr^{2+} sample. Thus, in the case of the presence of Eu^{3+}, the enhanced effect of light-induced electrons by Sr doping is hidden.

TABLE 1 Crystallographic parameters from GSASII X-ray Rietveld refinements of $Ca_{11.94-x}Sr_xAl_{14}O_{33}:Eu_{0.06}$ powders (x=0.00, 0.24, 0.48)

Sample	x=0.00	x=0.24	x=0.48
Space group	$I\bar{4}3d$	$I\bar{4}3d$	$I\bar{4}3d$
Crystal system	cubic	cubic	cubic
cell parameters			
a (Å)	11.9766 (3)	11.9788 (9)	11.9802 (0)
b (Å)	11.9766 (3)	11.9788 (9)	11.9802 (0)
c (Å)	11.9766 (3)	11.9788 (9)	11.9802 (0)
α (°)	90	90	90
β (°)	90	90	90
γ (°)	90	90	90
volume (Å^3)	1717.924	1718.897	1719.461
reliability factors			
R_{wp} (%)	11.70%	11.56%	10.77%
R_F^2	3.17%	5.63%	9.56%
χ^2	2.14	2.02	1.97

To elucidate the suppressed effect of light-induced electrons by the addition of Eu^{3+}, we study the photoluminescence property of $Ca_{11.94-x}Sr_xAl_{14}O_{33}:Eu_{0.06}$. The emission and excitation spectra of $Ca_{11.94-x}Sr_xAl_{14}O_{33}:Eu_{0.06}$ phosphors annealed in H_2 atmosphere are shown in Figure 3B and 4. From emission spectra, it can be observed that a strong and broad blue emission peak around 440 nm and several weak and sharp red emission peaks in the range 570-630 nm appear upon 254 nm excitation. They are ascribed to the 5d-4f transition of Eu^{2+} and the $^5D_0$-^7F_j (j=0, 1, 2) transitions of Eu^{3+}, respectively. From excitation spectra, two broad absorption bands (monitored at 440 nm) can be observed in the ranges 230-280 and 280-400 nm, which originate from the $4f^7$ ($^8S_{7/2}$)→$4f^65d^1$ (e_g) and $4f^7$ ($^8S_{7/2}$)→$4f^65d^1$ ($t_{2\ g}$) transitions of Eu^{2+} ions as given in Figure 4A.[38,39] Meanwhile, a broad band (in the range 220-280 nm) and several sharp peaks (in the range 310-550 nm) can be seen when monitoring the emission of Eu^{3+} at 613 nm, as shown in Figure 4B. The former is ascribed to the O_{2p}→Eu_{4f} charge-transfer (CT) transition and the sharp peaks at 320, 362, 383, 394, 415, 465, 526 and 533 nm are assigned to the transitions from the $^7F_0$ or $^7F_1$ state to the $^5H_4$, $^5D_4$, ^5G_J, $^5L_6$, $^5D_3$, $^5D_2$, and $^5D_1$ states of Eu^{3+}, respectively.[40] Since there exists the absorption overlaps of Eu^{2+} and Eu^{3+} in the range 230-280 nm, they can be simultaneously excited by a single wavelength UV light (like the above-mentioned 254 nm) to generate blue and red emissions.

In addition, it can be observed that the luminescence intensity of Eu^{2+} significantly increases, while the emission intensity of Eu^{3+} gradually decreases with increasing the

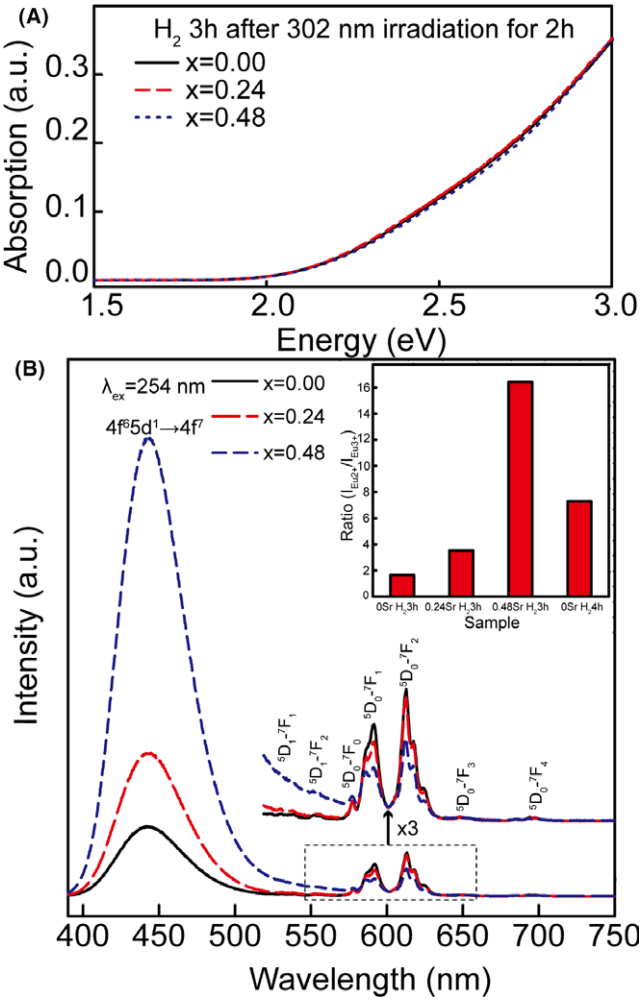

FIGURE 3 (A) The absorption spectra of $Ca_{11.94-x}Sr_xAl_{14}O_{33}:Eu_{0.06}$ phosphors (x=0.00, 0.24, 0.48) annealed at 1300°C for 3 h after 302 nm irradiation. (B) Emission (λ_{ex}=254 nm) spectra and the luminescence intensity ratio of Eu^{2+} to Eu^{3+} (the inset) of $Ca_{11.94-x}Sr_xAl_{14}O_{33}:Eu_{0.06}$ phosphors (x=0.00, 0.24, 0.48) annealed at 1300°C for different annealing times [Color figure can be viewed at wileyonlinelibrary.com]

Sr-doping concentration. Usually, the $^5D_0$→$^7F_1$ transition is a magnetic dipole transition, which is insensitive to the local environment around Eu^{3+} and the $^5D_0$→$^7F_2$ transitions is a forced electronic dipole transition, which is sensitive to the local environment around Eu^{3+}. Thus, the integrated intensity ratio of the $^5D_0$-$^7F_2$ to $^5D_0$-$^7F_1$ of Eu^{3+} (R_1) is an important parameter to characterize the change in the local environment around luminescent center. The higher ratio (R_1) is obtained, the lower symmetry is created.[41] In this work, for the undoped and Sr-doped samples (x=0.24, 0.48), the calculated R_1 values are 1.35, 1.54 and 2.08, respectively. The increased R_1 values indicate that the local environmental symmetry around Eu^{3+} becomes lower with increasing Sr-doping concentration. Thus, it will increase the radiative transition rate and enhance the luminescence intensity of Eu^{3+}.[34] However, the intensities of

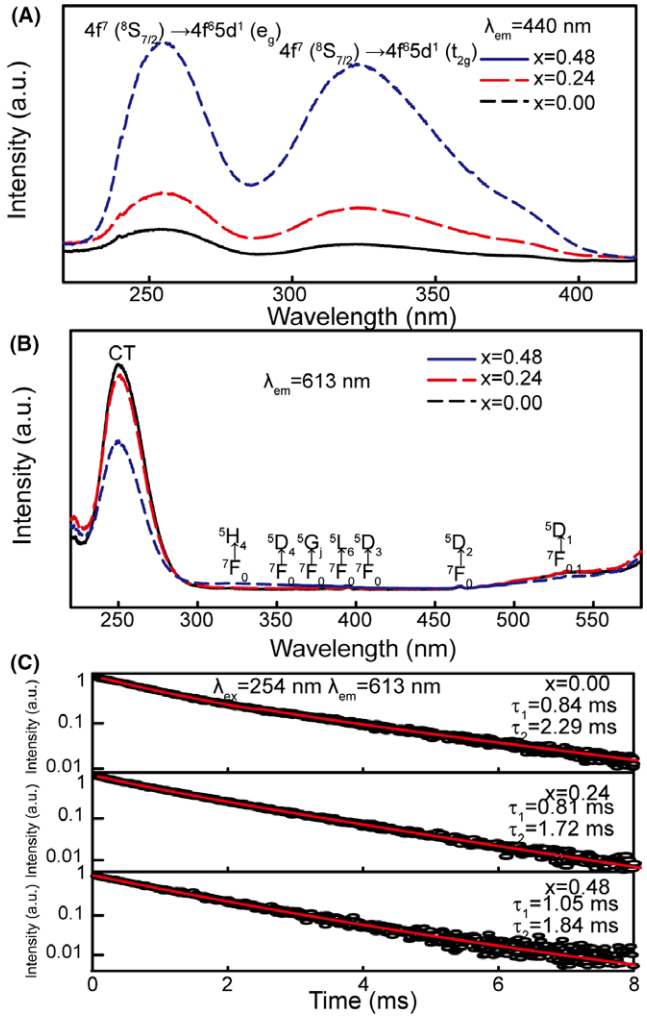

FIGURE 4 (A) Excitation spectra (A) (λ_{em}=440 nm) and (B) (λ_{em}=613 nm) of $Ca_{11.94-x}Sr_xAl_{14}O_{33}:Eu_{0.06}$ phosphors (x=0.00, 0.24, 0.48) annealed at 1300°C for 3 h. (C) Decay curves of Eu^{3+} monitoring at 613 nm excited at 254 nm for $Ca_{11.94-x}Sr_xAl_{14}O_{33}:Eu_{0.06}$ phosphors (x=0.00, 0.24, 0.48) annealed at 1300°C for 3 h. The red line represents the best fit to data using a bi-exponential function [Color figure can be viewed at wileyonlinelibrary.com]

Eu^{3+} decrease with increasing Sr-doping concentration. This abnormal behavior indicates that the remaining amount of Eu^{3+} is decreased and the reduction of Eu^{3+} to Eu^{2+} is enhanced after the introduction of Sr. Meanwhile, the luminescence decay curves of Eu^{3+} are shown in Figure 4C, the time constants of the three samples are almost the same. The time constants rely on radiative transition rate and the nonradiative transition. From the ratio of R_1 above, the radiative transition rate increase, so the nonradiative transition rate decrease to maintain the constants unchanged. If the nonradiative transition rate decrease, the luminescence intensity will increase. But the luminescence intensity of Eu^{3+} did not increase, we can conclude that remaining amount of Eu^{3+} is decreased. Thus, from the data of R_1 and the luminescence kinetics, more Eu^{2+} ions were generated after the introduction of Sr.

This result suggests that Sr doping can promote the reduction of Eu^{3+} to Eu^{2+} and suppress generation of light-induced electrons. In Eu^{3+}-doped $Ca_{12}Al_{14}O_{33}$, the reduction processes of Eu^{3+} to Eu^{2+} in H_2 atmosphere might be described in the following equations (3-6).

$$O_o^{\times} + 2Eu^{3+} \xrightarrow{2Ca^{2+}} 2Eu_{Ca}^{\cdot} + O^{2-}(\text{cage}) \quad (3)$$

$$O^{2-}(\text{cage}) \rightarrow \frac{1}{2}O_2(\text{gas}) + 2e' \quad (4)$$

$$2Eu_{Ca}^{\cdot} + 2e' \rightarrow 2Eu_{Ca}^{\times} \quad (5)$$

$$H_2(\text{gas}) + \frac{1}{2}O_2(\text{gas}) \rightarrow H_2O(\text{gas}) \quad (6)$$

where $O_o^{\times}$, O^{2-}(cage)and e'. stands for an empty nanocage, which is lost a encaged O^{2-}, encaged $O^{2-}$and an electron, respectively. In Equation (3), one encaged O^{2-}(with two negative charges) and two $Eu_{Ca}^{\cdot}$ will be simultaneously created after the replacement of two Ca sites by two Eu^{3+} ions. Encaged O^{2-} can be served as the donor of electrons as expressed in Equation (4), while two $Eu_{Ca}^{\cdot}$ become the acceptor of electrons as described in Equation (5). By the thermal activation, electrons provided by encaged O^{2-} will be generated on the surface of the grain of the sample, diffuse into the inside of the grain and trapped by $Eu_{Ca}^{\cdot}$. Thus the reduction of Eu^{3+} to Eu^{2+} is achieved followed by the evaporation of water (Equation 6). Meanwhile, it can be deduced that the consumption of encaged O^{2-} anions through Equation (3-6) restricts the forward reaction expressed in Equation (1). Therefore, the reduction of Eu^{3+} to Eu^{2+} limits the light-induced electrons in Eu-doped $Ca_{11.94-x}Sr_xAl_{14}O_{33}$ after irradiated with UV light. Meanwhile, with increasing the Sr-doping concentration, more Eu^{2+} ions are created. That is because O^{2-} lose electrons easily due to electronegativity of Sr is lower than Ca. On the other hand, when Ca is substituted by Sr, the larger entrance of nanocages (intercage opening) is produced. The schematic diagram of the nanocage entranceras for the undoped and Sr-doped phosphors is given in Figure 5A. Thus, the transmission of electrons is easier and the reduction of Eu^{3+} is enhanced.

To further confirm the suppressed generation of light-induced electrons by Sr doping, FTIR transmittance spectra of $Ca_{11.94-x}Sr_xAl_{14}O_{33}:Eu_{0.06}$ with different Sr dopant amounts are shown in Figure 5B. For the undoped sample, the spectrum exhibits an obvious peak at 3555 cm^{-1}, which originates from OH^- in $Ca_{12}Al_{14}O_{33}$. While the broad peak about 3426 cm^{-1} is ascribed to the water-absorption of the KBr transparent disk and $Ca_{12}Al_{14}O_{33}$ samples. For the Sr-doped samples, the peak intensities at 3555 cm^{-1} are similar after distracting the broad background. This result suggests that there does not exist the

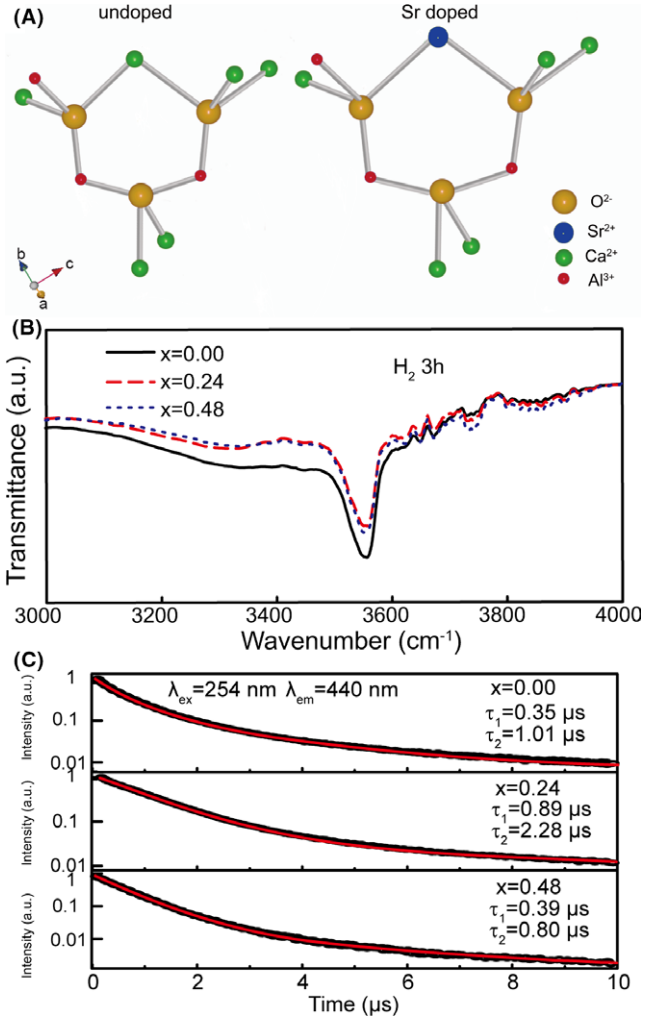

FIGURE 5 (A) The schematic diagram of the opening entrances of nanocages for the undoped and Sr-doped samples. (B) The FTIR transmittance spectra and (C) decay curves of Eu^{2+} monitoring at 440 nm excited at 254 nm for $Ca_{11.94-x}Sr_xAl_{14}O_{33}$:$Eu_{0.06}$ phosphors (x=0.00, 0.24, 0.48) annealed at 1300°C for 3 h. The red line represents the best fit to data, using a bi-exponential function [Color figure can be viewed at wileyonlinelibrary.com]

facilitated generation of encaged OH^- anions through Sr-doping strategy, which is different from the results in the Sr^{2+} and Gd^{3+} co-doped $Ca_{12}Al_{14}O_{33}$ powders. In that case, more encaged OH^- and H^- anions were generated as the Sr dopant amount increases through the reaction as expressed in Equation (1). However, our absorption and FTIR transmittance spectra suggest that no more encaged H^- and OH^- anions in the Sr-doped samples are created than that in the undoped sample. Our results indicate that there exists the suppressed effect of light-induced electrons by Sr doping due to the facilitated reduction of Eu^{3+} to Eu^{2+} in the case of the presence of Eu^{3+}.

Furthermore, the emission peak ratio of Eu^{2+} to Eu^{3+} (R_2) is used to evaluate the degree of the reduction of Eu^{3+} to Eu^{2+}. The larger R_2 means that more Eu^{2+} ions are reduced.[42] In our work, for the undoped (x=0.00) and Sr-doped samples (x=0.24, 0.48), the calculated emission peak ratios are 1.8, 3.6, and 16.4, respectively, as shown in the inset of Figure 3B. To further assess the dependence of the degree of the reduction of Eu^{3+} to Eu^{2+} on the Sr-doping concentration, the R_2 (~7.5) of the undoped powders annealed at 1300°C in H_2/N_2 atmosphere for 4 hours (as shown in the inset of Figure 3B) is used to compare with those of the Sr-doped samples annealed for 3 hours. It can be found that the R_2 value for x=0.48 increases by 1.3 times compared to that of the undoped sample annealed for longer time (4 hours).[34] Thus, Sr doping is more efficient for the reduction of Eu^{3+} to Eu^{2+}, which can be used for the application in the field of LED and FEDs.

To understand the variation of the local environment around Eu^{2+} with Sr dopant amount, Figure 5C shows the luminescence kinetics of Eu^{2+} in the $Ca_{11.94-x}Sr_xAl_{14}O_{33}$:$Eu_{0.06}$ samples (x=0.00, 0.24, 0.48) monitored at 440 nm upon 254 nm excitation. The fitting results are listed in Figure 5C. It can be found that each decay curve can be divided into two components corresponding to short and long lifetimes, respectively. The short lifetimes are in the range of 0.35-0.89 μs and the long lifetimes are in the range of 0.80-2.28 μs. Our previous study found that OH^- anions encaging $Ca_{12}Al_{14}O_{33}$ nanocages will promote non-radiative transition rates and shorten the lifetime.[18] Gao et al. reported these OH^- quenching centers lower the quantum efficiency of the doped ions.[43] Thus, the long and short lifetimes can be related to the local environments of O^{2-} and OH^- around Eu^{2+}, respectively. In particular, for the Sr-doped samples (x=0.48), the similar lifetimes compared to the undoped sample (x=0.00) indicate that Sr substitution does not lead to the obvious variation in the radiative and nonradiative transition rates of Eu^{2+}. The above result means that the enhanced luminescence intensity of Eu^{2+} originates from the increased amount of Eu^{2+} due to the facilitated reduction of Eu^{3+} to Eu^{2+} after Sr doping. The result is consistent with the explanation of the decreased intensity of Eu^{3+}, which has been demonstrated by the changes of R_1.

To evaluate the thermal stability of these caged phosphors, the relative emission intensities of the $Ca_{11.94-x}Sr_xAl_{14}O_{33}$:$Eu_{0.06}$ samples (x=0.00, 0.24, 0.48) as a function of temperature in the range of 298-473 K under 254 nm excitation are shown in Figure 6A-C. For the three samples, it is noted that their luminescence intensities decline with increasing temperature. This phenomenon is similar to that of Eu^{2+} doped in $Ca_{0.99}Y_{1-x}Al_{1-x}Si_xO_4$ reported by Zhang. et al.,[26] who have explained it by the thermally active phonon-assisted tunneling from the excited states of the lower-energy emission band to the high-vibration levels of the ground

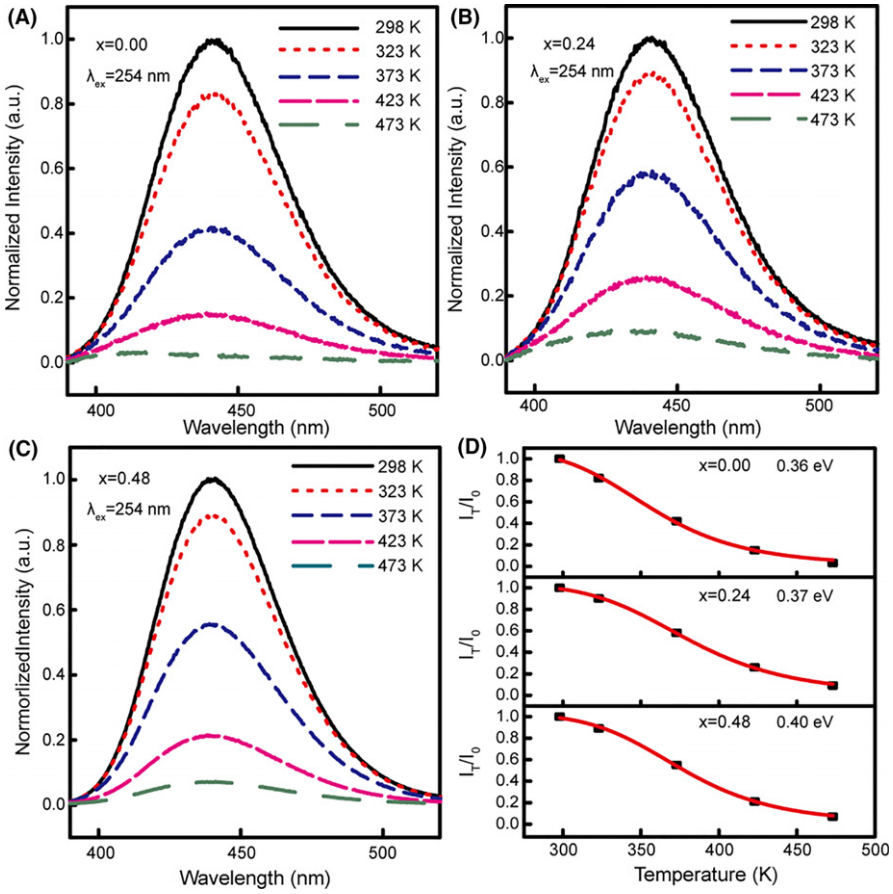

FIGURE 6 (A-C) Emission spectra of $Ca_{11.94-x}Sr_xAl_{14}O_{33}:Eu_{0.06}$ phosphors (x=0.00, 0.24, 0.48) as a function of temperature range from 298 to 473 K and (D) their temperature-dependent luminescence intensity as a function of temperature [Color figure can be viewed at wileyonlinelibrary.com]

state.[44] Usually, after Eu^{2+} ions absorb the excitation light, the emission happens at the bottom of the excited state followed by unwanted nonradiative transition.[45] At high temperature, the facilitated nonradiative relaxation occurs through the energy transfer at the crossing point between the ground and excited states, which could quench the luminescence.[27,44] To calculate the thermal activation energy, the emission intensity (I_T) of the $Ca_{11.94-x}Sr_xAl_{14}O_{33}:Eu_{0.06}$ samples (x=0.00, 0.24, 0.48) as a function of temperature are given in Figure 6D. Their emission intensities can be fitted by the following equation:

$$I_T/I_0 = [1 + D\exp(-E_a/kT)]^{-1} \quad (7)$$

where I_0, D and E_a represent the intensity at T=0 K, a constant and the thermal activation energy, respectively.[34] It can be found that the obtained E_a values are in the range of 0.36-0.40 eV and the thermal activation energy increases with increasing Sr-doping concentration. In general, it is assumed that the luminescent materials with high quenching temperature have rigid lattice. Therefore, our result indicates that the structure of $Ca_{11.94-x}Sr_xAl_{14}O_{33}$ becomes more rigid after Sr doping. This is because that the interaction between the encaged anions and the ions in the framework becomes weak due to the increased size of nanocages after Sr doping. The weaker the interaction becomes, the smaller the deformation of nanocages induces and the more rigid the framework structure becomes. The similar result has been reported by Tsai et al., who found that a rigid framework structure is created after Sr doping.[31] In addition, the emission intensity at 298 K of the Sr-doped sample (x=0.48) after the measurement at high temperatures is the same as that of the initial sample without the heat treatment, suggesting that there does not exist the oxidation of Eu^{2+} to Eu^{3+} in the temperature range of 298-473 K.

To explore the application of these caged phosphors for FEDs, CL spectra of the $Ca_{11.94-x}Sr_xAl_{14}O_{33}:Eu_{0.06}$ (x=0.00, 0.24, 0.48) phosphors under different electron beam accelerating voltages (accelerating voltage=1, 3, 5 kV, filament current=154 μA) are given in Figure 7A-C. It can be observed that the CL spectral shapes are similar to the PL ones and the CL intensities of Eu^{2+} increase rapidly with increasing the Sr-doping concentration. This can be explained by the increased amount of Eu^{2+} due to the enhanced reduction of Eu^{3+} to Eu^{2+} after Sr doping. In addition, the CL intensities of Eu^{2+} doped in the phosphors (x=0.00, 0.24, 0.48) increase linearly with increasing accelerating voltage from 1 to 5 kV, as shown in Figure 7D. Generally, the increase of CL intensities with increasing the accelerating voltage can be ascribed to the deeper

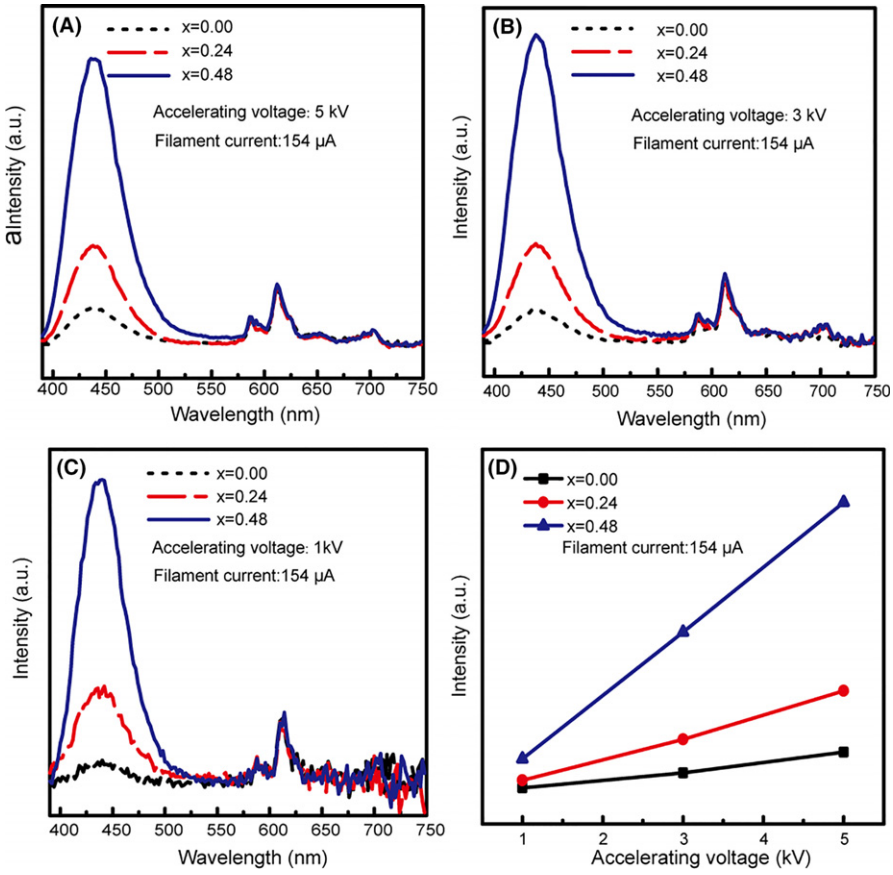

FIGURE 7 (A-C) CL spectra and (D) the CL intensities of $Ca_{11.94-x}Sr_xAl_{14}O_{33}$:$Eu_{0.06}$ phosphors (x=0.00, 0.24, 0.48) as a function of accelerating voltage under low-voltage (≤5 kV) electron beam excitation [Color figure can be viewed at wileyonlinelibrary.com]

penetration of the electrons into the phosphors body and the higher electron beam excitation density induced.[46] However, it is noted that the slope of the intensity-voltage curve becomes larger with increasing the Sr-doping concentration. The slope of the intensity-voltage curve is proportional to luminescence efficiency and the penetration depth. After Sr doping, the luminescence efficiency increases, which can be demonstrated by the ratio of R_1. Thus, the slope of the intensity-voltage curve becomes larger.

CIE coordinates of the $Ca_{11.94-x}Sr_xAl_{14}O_{33}$:$Eu_{0.06}$ phosphors (x=0.00, 0.24, 0.48) upon UV light (254 nm) and electron beam excitation (accelerating voltage=1 kV, filament current=154 μA) are shown in Figure 8. For the phosphors (x=0.00, 0.24, 0.48) upon 254 nm excitation, it can be found that their CIE coordinates are (0.537, 0.293), (0.456, 0.241) and (0.273, 0.125), respectively, and the colors of their emissions can be tuned from red to purple. For the phosphors (x=0.00, 0.24, 0.48) upon electron beam excitation, their CIE coordinates locate in (0.437, 0.197), (0.242, 0.113), and (0.187, 0.055), respectively, and the colors of their emissions are tuned from pink to blue. The difference CIE coordinates of the same phosphor upon UV light and electron beam excitations might be related to the different excitation efficiencies of Eu^{3+} and Eu^{2+}.[37] Our results suggest that strontium doping is an efficient strategy

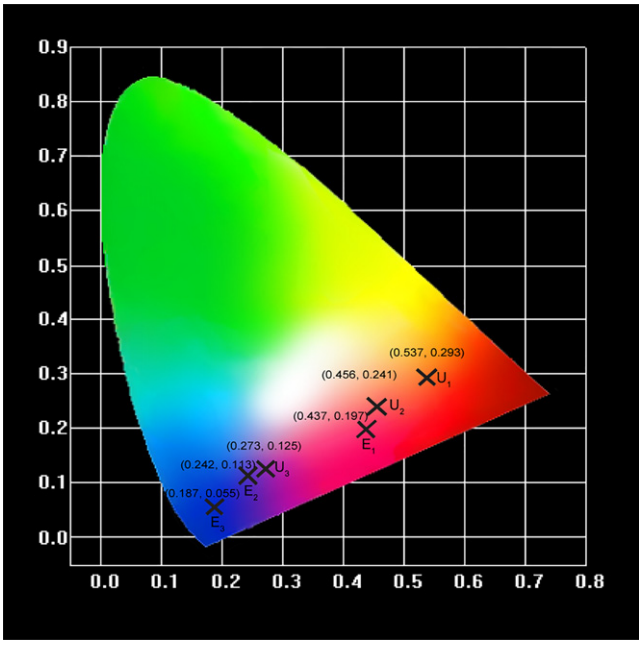

FIGURE 8 CIE chromaticity coordinates of $Ca_{11.94-x}Sr_xAl_{14}O_{33}$:$Eu_{0.06}$ phosphors (x=0.00, 0.24, 0.48) under 254 nm and electron beam excitation (accelerating voltage=1 kV) [Color figure can be viewed at wileyonlinelibrary.com]

for enhancing the reduction of Eu^{3+} to Eu^{2+} and the $Ca_{11.94-x}Sr_xAl_{14}O_{33}$:$Eu_{0.06}$ phosphors might be a candidate for lighting and flat-panel displays.

4 | CONCLUSIONS

In conclusion, europium-doped $Ca_{11.94-x}Sr_xAl_{14}O_{33}$ phosphors with cage-like structure were prepared by a self-propagating combustion method followed by thermal annealing in H_2 atmosphere. The absorption spectra and FTIR transmittance spectra of the phosphors with different Sr dopant amounts confirm that there exists the suppressed generation of encaged H^- and OH^- anions by Sr doping. It can be found that the enhanced effect of light-induced electrons by Sr doping is hidden by the addition of Eu^{3+}. Our results suggest that strontium doping enhances the reduction of Eu^{3+} to Eu^{2+} in $Ca_{11.94-x}Sr_xAl_{14}O_{33}:Eu_{0.06}$ phosphors. The obtained higher thermal activation energy of the Sr-doped sample can be attributed to the more rigid framework structure after Sr doping. For the phosphors with different Sr dopant amounts, the emission colors are tuned from red to purple upon 254 nm excitation and from pink to blue under electron beam excitation. The insight gained from this work is help for designing and developing novel nanocaged phosphors for LED and FEDs.

ACKNOWLEDGMENTS

This work was supported by the National Natural Science Foundation of China (No. 11374047, No.11674050 & No. 11304036), European union MSCA-ITN-2015-ETN Action program, ISPIC, under grant nr. 675742 and Netherlands Organisation for Scientific Research in the framework of the Fund New Chemical Innovation (2015) TA under grant nr. 731.015.206.

REFERENCES

1. Ellis-Davies GC. Caged compounds: photorelease technology for control of cellular chemistry and physiology. *Nat Methods*. 2007;4:619-628.
2. Mastalerz M, Schneider MW, Oppel IM, Presly O. A salicylbisimine cage compound with high surface area and selective CO_2/CH_4 adsorption. *Angew Chem Int Ed*. 2011;50:1046-1051.
3. Richers MT, Amatrudo JM, Olson JP, Ellis-Davies GC. Cloaked caged compounds: chemical probes for two-photon optoneurobiology. *Angew Chem Int Ed*. 2016;55:1-6.
4. Kitano M, Inoue Y, Yamazaki Y, et al. Ammonia synthesis using a stable electride as an electron donor and reversible hydrogen store. *Nature Chem*. 2012;4:934-940.
5. Kamiya T, Aiba S, Miyakawa M, et al. Field-induced current modulation in nanoporous semiconductor, electron-doped $12CaO{\cdot}7Al_2O_3$. *Chem Mater*. 2005;17:6311-6316.
6. Irvine J, West A. $Ca_{12}Al_{14}O_{33}$—a possible high-temperature moisture sensor. *J Appl Electrochem*. 1989;19:410-412.
7. Schmidt A, Lerch M, Eufinger J-P, et al. Chlorine ion mobility in Cl-mayenite ($Ca_{12}Al1_4O_{32}Cl_2$): an investigation combining high-temperature neutron powder diffraction, impedance spectroscopy and quantum-chemical calculations. *Solid State Ionics*. 2014;254:48-58.
8. Matsuishi S, Toda Y, Miyakawa M, et al. High-density electron anions in a nanoporous single crystal:$[Ca_{24}Al_{28}O_{64}]^{4+}(4e^-)$. *Science*. 2003;301:626-629.
9. Sushko PV, Shluger AL, Hayashi K, Hirano M, Hosono H. Electron localization and a confined electron gas in nanoporous inorganic electrides. *Phys Rev Lett*. 2003;91:12401.
10. Sushko P, Shluger A, Hayashi K, Hirano M, Hosono H. Mechanisms of oxygen ion diffusion in a nanoporous complex oxide $12CaO{\bullet}7Al_2O_3$. *Phys Rev B*. 2006;73:014101.
11. Strandbakke R, Kongshaug C, Haugsrud R, Norby T. High-temperature hydration and conductivity of mayenite, $Ca12Al14O_{33}$. *J Phys Chem C*. 2009;113:8938-8944.
12. Hayashi SMK, Kamiya T, Hirano M, Hosono H. Light-induced conversion of an insulating refractory oxide into a persistent electronic conductor. *Nature*. 2002;419:462-465.
13. Hayashi SMK, Hirano M, Hosono H. Hydride ion as photoelectron donor in microporous crystal. *J Am Chem Soc*. 2005;127:12454-12455.
14. Hayashi K. Heavy doping of H^- ion in 12CaO·7Al2O3. *J Solid State Chem*. 2011;184:1428-1432.
15. Jeevaratnam J, Glasser F, Glasser LD. Anion substitution and structure of 12CaO·7A12O3. *J Am Chem Soc*. 1964;47:105-106.
16. Schmidt A, Lerch M, Eufinger J-P, et al. CN-mayenite $Ca_{12}Al_{14}O_{32}(CN)_2$: replacing mobile oxygen ions by cyanide ions. *Solid State Sci*. 2014;38:69-78.
17. Miyakawa M, Hiramatsu H, Kamiya T, Hirano M, Hosono H. Fabrication and electron transport properties of epitaxial films of electron-doped $12CaO{\cdot}7Al_2O_3$ and $12SrO{\cdot}7Al_2O_3$. *J Solid State Chem*. 2010;183:385-391.
18. Zhang M, Liu Y, Zhu H, et al. Enhancement of encaged electron-concentration by Sr^{2+} doping and improvement of Gd^{3+} emission through controlling encaged anions in conductive C12A7 phosphors. *Phys Chem Chem Phys*. 2016;18:18697-18704.
19. Sun C, Pratx G, Carpenter CM, et al. Synthesis and radioluminescence of PEGylated Eu^{3+}-doped nanophosphors as bioimaging probes. *Adv Mater*. 2011;23:H195-H199.
20. Yao M, Chen W. Hypersensitive luminescence of Eu^{3+} in dimethyl sulfoxide as a new probing for water measurement. *Anal Chem*. 2011;83:1879-1882.
21. Attia M, Essawy AA, Youssef A, Mostafa MS. Determination of ofloxacin using a highly selective photo probe based on the enhancement of the luminescence intensity of Eu^{3+}—ofloxacin complex in pharmaceutical and serum samples. *J Fluoresc*. 2012;22:557-564.
22. Gupta SK, Rajeshwari B, Achary S, et al. Europium luminescence as a structural probe: structure-dependent changes in Eu^{3+}-substituted $Th(C_2O_4)_2\ xH_2O$ (x= 6, 2, and 0). *Eur J Inorg Chem*. 2015;2015:4429-4436.
23. Xie Y, Perera TSH, Li F, Han Y, Yin M. Quantitative detection method of hydroxyapatite nanoparticles based on Eu^{3+} fluorescent labeling in vitro and in vivo. *ACS Appl Mater Interfaces*. 2015;7:23819-23823.
24. Liu Y, Zhou S, Zhuo Z, et al. In vitro upconverting/downshifting luminescent detection of tumor markers based on Eu^{3+}-activated core–shell–shell lanthanide nanoprobes. *Chem Sci*. 2016;7:5013-5019.
25. Rohwer LES, McKittrick J. Review: down conversion materials for solid state lighting. *J Am Ceram Soc*. 2014;97:1327-1352.

26. Zhang Y, Li X, Li K, Lian H, Shang M, Lin J. Crystal-site engineering control for the reduction of Eu^{3+} to Eu^{2+} in $CaYAlO_4$: structure refinement and tunable emission properties. *ACS Appl Mater Interfaces*. 2015;7:2715-2725.
27. Liu C, Qi Z, Ma C-G, et al. High light yield of $Sr_8(Si_4O_{12})Cl_8$: Eu^{2+} under x-ray excitation and its temperature-dependent luminescence characteristics. *Chem Mater*. 2014;26:3709-3715.
28. Pust P, Wochnik AS, Baumann E, et al. Ca $[LiAl_3N_4]$: Eu^{2+} a narrow-band red-emitting nitridolithoaluminate. *Chem Mater*. 2014;26:3544-3549.
29. Takeda T, Hirosaki N, Funahshi S, Xie R-J. Narrow-band green-emitting phosphor $Ba_2LiSi_7AlN_{12}$:Eu^{2+} with high thermal stability discovered by a single particle diagnosis approach. *Chem Mater*. 2015;27:5892-5898.
30. Park WBS, Singh SP, Sohn K-S. Discovery of a phosphor for light emitting diode applications and its structural determination, $Ba(Si, Al)_5(O, N)8:Eu^{2+}$. *J Am Chem Soc*. 2014;136:2363-2373.
31. Tsai Y-T, Chiang C-Y, Zhou W, Lee J-F, Sheu H-S, Liu R-S. Structural ordering and charge variation induced by cation substitution in (Sr, Ca)$AlSiN_3$: Eu phosphor. *J Am Chem Soc*. 2015;137:8936-8939.
32. Toby BH, Von Dreele RB. GSAS-II: the genesis of a modern open-source all purpose crystallography software package. *J Appl Crystallogr*. 2013;46:544-549.
33. Katsuro Hayashi PVS, Shluger AL, Hirano M, Hosono H. Hydride ion as a two-electron donor in a nanoporous crystalline semiconductor. *J Phys Chem B*. 2005;109:23836-23842.
34. Bian H, Liu Y, Yan D, et al. Spectral modulation through controlling anions in nanocaged phosphors. *J Mater Chem C*. 2013;1:7896-7903.
35. Liu X, Liu Y, Yan D, et al. Single-phased white-emitting $12CaO{\cdot}7Al_2O_3$:Ce3+, Dy^{3+} phosphors with suitable electrical conductivity for field emission displays. *J Mater Chem*. 2012;22:16839-16843.
36. Liu X, Liu Y, Yan D, et al. A multiphase strategy for realizing green cathodoluminescence in $12CaO{\cdot}7Al_2O_3$-$CaCeAl_3O_7$:Ce^{3+}, Tb3+ conductive phosphor. *Dalton Trans*. 2013;42:16311-16317.
37. Zhang X, Liu Y, Zhang M, et al. Red-emitting nano-porous $12CaO\ 7Al_2O_3$: Sm^{3+} conductive phosphor for low-voltage field emission displays. *Mater Res Bull*. 2017;86:51-56.
38. Zeuner M, Hintze F, Schnick W. Low temperature precursor route for highly efficient spherically shaped LED-phosphors $M_2Si_5N_8$:Eu^{2+} (M = Eu, Sr, Ba). *Chem Mater*. 2009;21:336-342.
39. Zeuner M, Schmidt PJ, Schnick W. One-pot synthesis of single-source precursors for nanocrystalline LED phosphors $M_2Si_5N_8$:Eu^{2+} (M = Sr, Ba). *Chem Mater*. 2009;21:2467-2473.
40. Gao G, Reibstein S, Peng M, Wondraczek L. Tunable dual-mode photoluminescence from nanocrystalline Eu-doped Li_2ZnSiO_4 glass ceramic phosphors. *J Mater Chem*. 2011;21:3156-3161.
41. Yiguo Su LL, Guangshe L. Synthesis and optimum luminescence of $CaWO_4$ based red phosphors with codoping of Eu^{3+} and Na^{+}". *Chem Mater*. 2008;20:6060-6067.
42. Zhang J-C, Long Y-Z, Zhang H-D, Sun B, Han W-P, Sun X-Y. Eu^{2+}/Eu^{3+}-emission-ratio-tunable $CaZr(PO_4)_2$: Eu phosphors synthesized in air atmosphere for potential white light-emitting deep UV LEDs. *J Mater Chem C*. 2014;2:312-318.
43. Chang-Cheng G, Shi-Hua H, Fang-Tian Y, Kai K, Ying F. Influence of surface quenching effects on luminescent dynamics of ZnS: Mn^{2+} nanocrystals. *Chin Phys Lett*. 2008;25:698-699.
44. Ci Z, Que M, Shi Y, Zhu G, Wang Y. Enhanced photoluminescence and thermal properties of size mismatch in $Sr_{2.\ 97-x-y}Eu_{0.\ 03}Mg_{\ x}Ba_ySiO_5$ for high-power white light-emitting diodes. *Inorg Chem*. 2014;53:2195-2199.
45. Li G, Lin CC, Chen W-T, et al. Photoluminescence tuning via cation substitution in oxonitridosilicate phosphors: DFT calculations, different site occupations, and luminescence mechanisms. *Chem Mater*. 2014;26:2991-3001.
46. Zhang Q-H, Wang J, Yeh C-W, et al. Structure, composition, morphology, photoluminescence and cathodoluminescence properties of $ZnGeN_2$ and $ZnGeN_2$: Mn^{2+} for field emission displays. *Acta Mater*. 2010;58:6728-6735.

How to cite this article: Bian H, Liu Y, Yan D, et al. Light-induced electrons suppressed by Eu^{3+} ions doped in $Ca_{11.94-x}Sr_xAl_{14}O_{33}$ caged phosphors for LED and FEDs. *J Am Ceram Soc*. 2017;100:3467–3477. https://doi.org/10.1111/jace.14866